Surface & Coatings Technology 206 (2012) 5036–5041

Contents lists available at SciVerse ScienceDirect

Surface & Coatings Technology

journal homepage: www.elsevier.com/locate/surfcoat

Inhibited aluminization of an ODS FeCr alloy

A. Rouaix-Vande Put [1], B.A. Pint *

Materials Science and Technology Division, Oak Ridge National Laboratory, Oak Ridge, TN 37831-6156, USA

ARTICLE INFO

Article history:
Received 4 January 2012
Accepted in revised form 12 May 2012
Available online 19 May 2012

Keywords:
Chemical vapor deposition
Aluminide coatings
ODS alloys
Ferritic steels
Fusion energy

ABSTRACT

Aluminide coatings are of interest for fusion energy applications both for compatibility with liquid Pb–Li and to form an alumina layer that acts as a tritium permeation barrier. Oxide dispersion strengthened (ODS) ferritic steels are a structural material candidate for commercial reactor concepts expected to operate above 600 °C. Aluminizing was conducted in a laboratory scale chemical vapor deposition reactor using accepted conditions for coating Fe- and Ni-base alloys. However, the measured mass gains on the current batch of ODS Fe–14Cr were extremely low compared to other conventional and ODS alloys. After aluminizing at two different Al activities at 900 °C and at 1100 °C, characterization showed that the ODS Fe–14Cr specimens formed a dense, primarily AlN layer that prevented Al uptake. This alloy batch contained a higher (>5000 ppma) N content than the other alloys coated and this is the most likely reason for the inhibited aluminization. Other factors such as the high O content, small (~140 nm) grain size and Y–Ti oxide nano-clusters in ODS Fe–14Cr also could have contributed to the observed behavior. Examples of typical aluminide coatings formed on conventional and ODS Fe- and Ni-base alloys are shown for comparison.

1. Introduction

The present focus of the U.S. fusion materials program is to address issues associated with the dual coolant Pb–Li (DCLL) blanket concept [1] for a test blanket module (TBM) for ITER and enhanced concepts for a DEMO-type fusion reactor leading to commercial power production. A DCLL blanket has both He and eutectic Pb–Li coolants and uses reduced activation ferritic–martensitic (FM) steel [2] as the structural material with a SiC/SiC composite flow channel insert (FCI). Thus, recent U.S. compatibility research has examined compatibility issues of these materials with the Pb–Li coolant [3–7]. Compared to Li [8,9], a wider range of materials can be compatible with Pb–Li because of the low activity of Li in the eutectic composition [10]. In particular, SiC and α-Al_2O_3 readily dissolve in Li, but not in Pb–17Li [3,4,9,11]. However, because of higher Ni and Fe solubilities, Pb–Li readily dissolves many conventional alloys above 500 °C [12]. This is not a concern for a DCLL TBM operating in ITER at <500 °C, however, a DCLL blanket for a commercial reactor would be more attractive with a higher maximum operating temperature, perhaps >600 °C if oxide dispersion strengthened (ODS) ferritic (or ODS FM) steels [13,14] were used. Even at 550 °C, a recent study of FM Eurofer 97 (Fe–Cr–W) showed a very high dissolution rate in flowing Pb–Li [15]. Therefore, several strategies are being explored to reduce the FM steel dissolution rate at ≥500 °C. Preliminary isothermal Pb–Li compatibility capsule experiments are being conducted at 500°–800 °C in order to investigate mitigation strategies before flowing Pb–Li compatibility tests are conducted [3–7].

One of the most promising strategies is Al additions either to the alloy or as an aluminide or Al-rich coating, which form a stable, protective Al-rich oxide that inhibits alloy dissolution in Pb–Li [3–7,16–18]. Such coatings have shown dramatically lower mass losses in 1000 h Pb–Li capsule tests than conventional FM alloys without Al, Fig. 1. Aluminide coatings have been evaluated for both their corrosion resistance and as tritium permeation barriers, particularly when the aluminide coating is used to form an external, thermally-grown alumina scale with very low tritium permeation [17,19–21]. Tritium management is a critical issue in fusion reactors as its generation in the blanket provides the fuel for the D-T fusion reaction [22]. The results in Fig. 1 show low mass changes after Pb-Li exposures of Al-rich coatings made by chemical vapor deposition (CVD) on conventional and commercial ODS alloys in a laboratory-scale reactor [23,24]. The CVD process has been used to make high purity reproducible Al-rich coatings for these laboratory studies and likely would be replaced by another coating process (e.g. slurry coating) for commercially coating large reactor components. However, it has not been possible to CVD aluminize an ODS Fe–14Cr alloy (14YWT) that is a leading structural material candidate for fusion reactors because ODS alloys have an exceptional combination of creep strength and radiation damage resistance [14,25–27]. Characterization of 14YWT specimens after exposure in the CVD reactor under three different aluminizing conditions are presented and compared to other alloys after similar exposures. A possiblemechanism for the inhibited aluminization has been identified.

* Corresponding author. Tel.: +33 865 576 2897.
E-mail address: pintba@ornl.gov (BA. Pint).
[1] Current address: Institut Carnot CIRIMAT, ENSIACET, 4 allée Emile Monso, BP 44362, 31432 Toulouse Cedex 4, France.

0257-8972/$ – see front matter © 2012 Elsevier B.V. All rights reserved.
doi:10.1016/j.surfcoat.2012.05.041

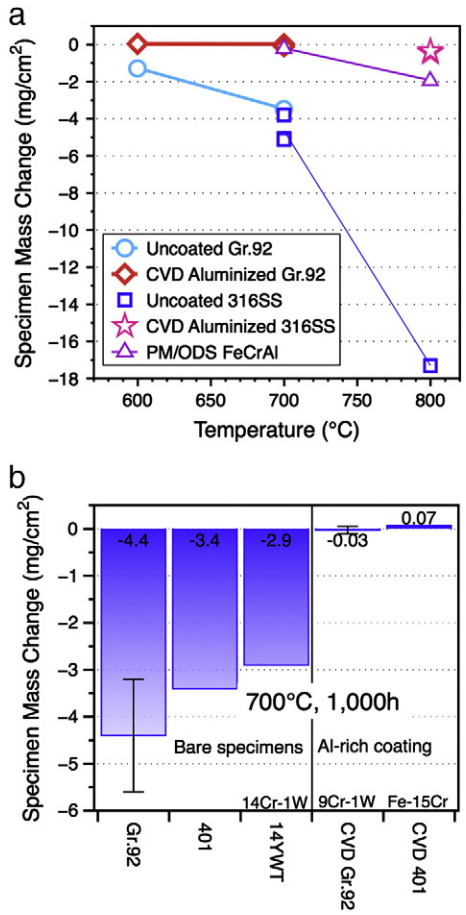

Fig. 1. Specimen mass loss in Pb–Li for 1000 h in Mo capsules, (a) as a function of exposure temperature and (b) at 700 °C comparing ODS and wrought alloys with and without coatings (standard deviation bars where the bar is an average when two specimens were exposed). Powder metallurgy (PM) or ODS alumina-forming alloys or Al-rich coatings have much lower mass losses than conventional Fe-base alloys [3–7].

2. Experimental procedure

The composition and grain sizes of the alloys aluminized in this study are given in Table 1. The ODS Fe–14Cr is made using high energy ball milling and warm extrusion and the details are presented elsewhere [26]. This particular batch of ODS Fe–14Cr material used in these experiments (SM10) had a very fine grain size (~140 nm). Prior to coating, specimens were polished to a 0.3 μm alumina finish and cleaned ultrasonically in acetone and alcohol. Aluminizing was performed in a laboratory-scale CVD reactor consisting of an inductively heated alumina tube typically with flowing H_2 (300 cm^3/min) and HCl (20 cm^3/min) creating $AlCl_x$ vapor from Al pellets. The reactor has been described in detail elsewhere [23,24]. In these experiments, typically four specimens were hung from two alumina rods perpendicular to the flowing gas stream and are designated front or back with relation to the flow. The front specimens typically had 10–30% higher mass gain. In addition to the Al powder, Al–60wt.%Cr powder was added to the reactor to increase the Al activity for some runs at 900 °C, but not at 1100 °C [24]. The specimen mass change was measured before and after aluminizing with an accuracy of ±0.01 mg/cm^2. A summary of the conditions and mass change data for each of the ODS specimens is given in Table 2. After aluminizing, the specimens were examined by light microscopy, X-ray diffraction (XRD), a K-Alpha X-ray photoelectron spectrometer (XPS) and a Hitachi model S4800 scanning electron microscopy (SEM). For cross-sectioning, standard metallographic techniques were used or a Hitachi model NB5000 focused ion beam (FIB) for thin reaction products.

Table 2
Mass change of ODS specimens in CVD aluminizing for 6 h in laboratory reactor.

Specimen	Temperature (°C)	Powder	Location	Mass change (mg/cm^2)
14YWT	1100°	No	Front	−0.61
	900°	Al/Cr	Front	0.05
				0.06
				0.15
		No	Back	0.02
754 (NiCr)	1100°	No	Front	8.02
	900°	Al/Cr	Back	1.54
401 (FeCr)	900°	No	Back	1.30

3. Results

The average mass gain data for the two CVD aluminizing temperatures are shown in Figs. 2 and 3 and the data for the ODS alloys are summarized in Table 2. In both figures, the number of specimens in the average is shown above each bar. The comparison mass gain data are from a variety of different projects that have made coatings for fossil energy applications in the same CVD reactor [29–31]. At 900 °C, the mass gain for the 14YWT material was much lower than

Table 1
Alloy chemical compositions (atomic% or ppma) determined by inductively coupled plasma analysis and combustion analysis and alloy grain size.

Material	Fe %	Ni %	Cr %	Al %	O ppma	C ppma	N ppma	S ppma	Other %	Grain size (μm)
14YWT	83.3	0.03	14.1	0.04	6000	3000	**5170**	69	0.59W,0.12Y 0.28Ti,0.08Si	0.14
401	82.6	0.12	14.8	0.12	6560	610	1770	89	0.17Mo,0.13Y 1.2Ti,0.08Si	0.5×1–3[a] [28]
Gr.91 (9Cr–1Mo)	87.8	0.1	9.9		90	2380	**1900**	14	0.6Mo,0.3V, 0.5Mn,0.4Si,	~20
Gr.92 (9Cr–1W)	87.2	0.1	9.9	0.02	80	5120	**2330**	87	0.55W,0.46Mn 0.30Mo,0.32Si	~20
754	0.4	75.3	20.6	0.7	15,600	2900	3520	9	0.50Ti,0.27Y	>1000
740	2.0	46.2	25.3	1.7	60	3650	460	<	19.3Co,2,3Ti,1.2Nb 0.9Si,0.3Mn,0.3Mo	~50
X	18.7	46.5	24.8	0.2	33	3260	1680	<	5.8Mo,1.8Co 0.2W,0.7Mn,0.6Si	~50
N5	0.1	64.8	7.8	13.9	52	2490	<	7	7.3Co,2.1Ta,1.6W 1Re,0.9Mo,0.05Hf,0.003Y	n.a.[b]

< indicates below the detectability limit of <0.01% or <0.001% for interstitials.
[a] Grains elongated in the extrusion direction which was parallel to the coated faces.
[b] Single crystal alloy.

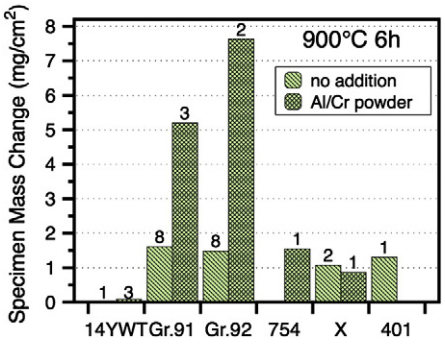

Fig. 2. Average specimen mass change after 6 h at 900 °C in a laboratory-scale CVD reactor with and without Al–Cr powder to raise the Al activity and increase the Al uptake. The numbers mark the number of specimens exposed.

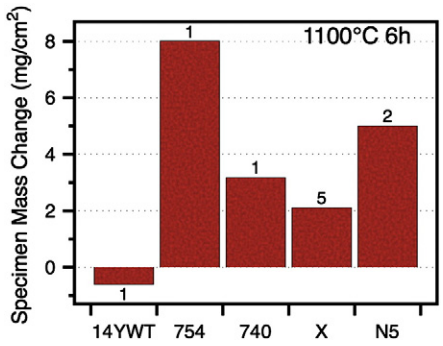

Fig. 3. Average specimen mass change after 6 h at 1100 °C in a laboratory-scale CVD reactor. The numbers mark the number of specimens exposed.

other FM steels (Grades 91 and 92) at 900 °C and even lower than the ODS and wrought commercial austenitic Ni-base alloys (754 and X). Because of the slower Al diffusivity in austenite compared to the ferritic alloys, it is expected that the mass gains will be lower. Typically, Ni-base alloys are aluminized at higher temperatures, than Fe-base alloys. At 900 °C, the mass gain was slightly higher for the 14YWT specimens when Al–Cr powder was added to the reactor but still more than an order of magnitude lower than all of the comparison materials. At 1100 °C, the 14YWT specimen lost mass while the Ni-base alloys all gained mass, forming a NiAl coating [23,30]. No other Fe-base alloys were aluminized at 1100 °C as the coating would be very thick (>250 μm) [24].

One commercial ODS FeCr alloy (401)[28] was previously aluminized at 900 °C without powder and showed a mass gain similar to Grades 91 and 92, Fig. 2. The coated 401 specimen was not sectioned after coating but was exposed to Pb–Li at 700 °C, showing the effectiveness of the coating, Fig. 1b. Because of the limited availability of other ODS FeCr alloys to compare to 14YWT, an ODS NiCr alloy, 754 (commercially designated MA754 by manufacturer Special Metals), was included in two runs adjacent to the 14YWT specimen for a direct comparison. At both temperatures, the 754 specimen mass gain was significantly higher than the 14YWT specimen, gaining more mass than the comparable wrought (X) or cast (N5) Ni-base alloys at 900° and/or 1100 °C, Table 2 and Figs. 2 and 3.

In order to determine why the 14YWT specimen did not gain mass during aluminizing, the characterization compared the 14YWT and 754 specimens, as both are dispersion-strengthened alloys. Figs. 4 and 5 show the surface morphology of both materials after aluminizing. For Ni-base alloys, the morphology of 754 after 6 h at 1100 °C, Fig. 5c, is a typical aluminized morphology with NiAl coating grain boundaries clearly evident and slight ridges forming on most boundaries [23,29]. At 900 °C, the aluminide grains appear to be finer on 754 with similar grain boundary ridges, Fig. 4c. In contrast, the surface of 14YWT at both temperatures was much different with fewer distinctive features, Figs. 4a and 5a. Higher magnification images of the 14YWT surface are shown in Figs. 4b and 5b that suggest a much finer grained surface layer, nothing like an aluminide structure.

Based on the low mass change and surface morphology for 14YWT, a thin reaction product was expected that could be studied by a surface analytical technique such as XPS. Fig. 6 shows sputter depth profiles for 14YWT after CVD exposures at 900° (with powder) and 1100 °C. The sputter depth is estimated based on a calibration with the sputter crater depth. At 900 °C, the surface is rich in Al, O and N with the O signal falling off faster than the N signal. Based on the crossover of the Fe and Al signals, this outer Al-rich oxy-nitride layer appears to be less than 100 nm in thickness. The Al signal drops to background levels by 175 nm. Typically, FM steels aluminized under these conditions would show ~32–36 at.%Al at the surface with an Al profile extending 100 μm into the substrate [7]. Such deep Al profiles were observed with coating mass gains of 5–7 mg/cm^2, Fig. 2. At 1100 °C, the reaction product on 14YWT was much thicker and appeared to be more concentrated in N than at 900 °C, Fig. 6b. Again based on the Al–Fe signal crossover, the surface reaction product appeared to be ~700 nm thick. The composition change at ~250 μm depth is where the XPS sputtering was stopped and then restarted at the same location. The formation of this surface AlN layer on 14YWT is not consistent with the mass loss observed

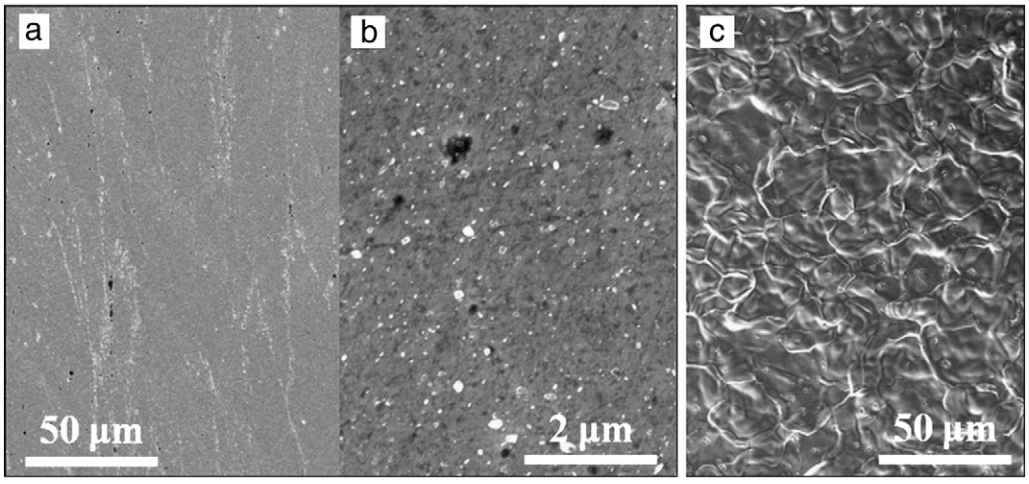

Fig. 4. SEM plan view images of the specimen surface after aluminizing for 6 h at 900 °C with Al–Cr powder (a,b) 14YWT and (c) 754.

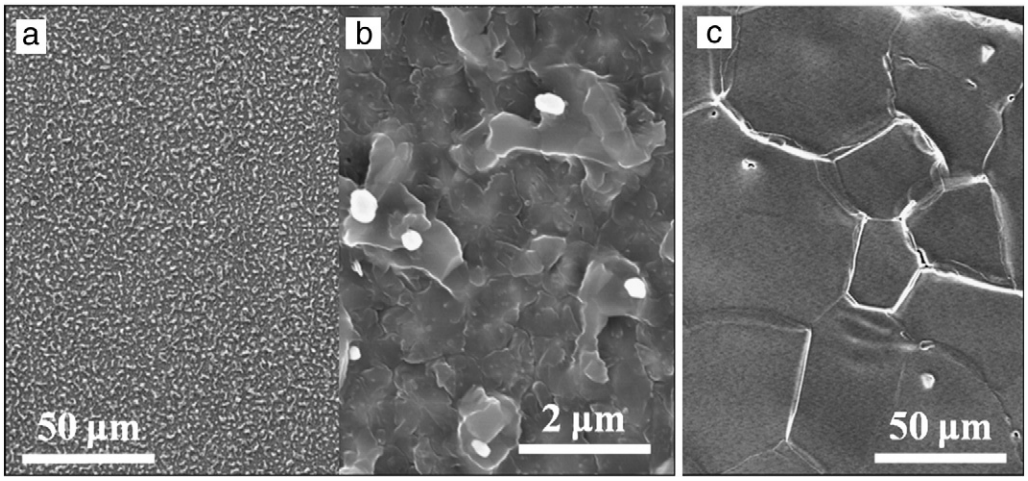

Fig. 5. SEM plan view images of the specimen surface after aluminizing for 6 h at 1100 °C (a,b) 14YWT and (c) 754.

after exposure, Table 2. One possibility is that some Fe was removed from the surface by the Cl in the environment, as suggested by Kung and Rapp [32]. The reaction layer on 14YWT after the 1100 °C CVD exposure was further characterized by XRD to confirm the presence of a nitride layer. Fig. 7 shows the XRD spectrum with peaks from the ferritic matrix and AlN labeled.

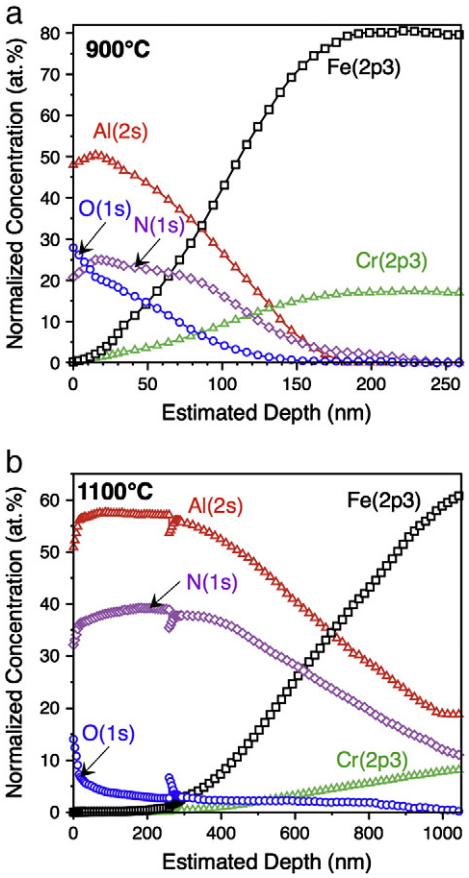

Fig. 6. XPS sputter depth profiles of 14YWT after aluminizing at (a) 900 °C with powder and (b) 1100 °C. The outer surface is rich in Al, O and N in both cases. In (b), the signal change at ~250 µm is where the sputtering was stopped and restarted in the same location.

The surface of the aluminized 754 specimens also was sputtered by XPS for comparison. Fig. 8 shows that after both CVD temperatures, a ~10 nm oxide layer was detected on the surface of the aluminide layer with some C present. This is more typical of the native oxide expected on a CVD aluminized substrate.

To characterize the coatings formed on the other alloys, Figs. 9 and 10 show example cross-sections on representative alloys (examples for coatings on other alloys can be found elsewhere [23,24,30]). Figs. 9c and 10a show the coating formed on 754 after CVD aluminizing at 900° with Al–Cr powder and 1100 °C, respectively. For the 14YWT specimens coated in the same CVD exposures, no coating was evident, Figs. 9d and 10b. The 1100 °C coating on 754 is typical of all Ni-base alloys with an outer NiAl layer and an underlying interdiffusion zone. A similar structure was observed on alloy X at 900 °C, Fig. 9a. The 900 °C coating with Al–Cr powder on 754 had a somewhat different structure, perhaps due to the higher Al activity, Fig. 9c.

To better characterize the thin layer formed on 14YWT after aluminizing at 1100 °C, Fig. 11 shows a cross-section of the reaction product prepared by FIB sectioning. A W coating was deposited on the surface to protect the reaction product during sectioning by the ion beam. In this region, the reaction product appears to be continuous and at least 250 nm thick, less than that suggested by the XPS sputtering profile. However, quantifying the sputtering rate can be difficult and may have overestimated the AlN thickness. Also, the layer thickness may not be uniform on the specimen. This layer acted as a solid-state

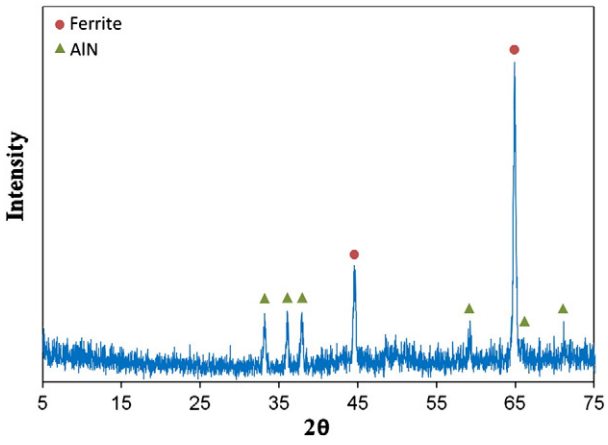

Fig. 7. XRD spectra from 14YWT after CVD exposure at 1100 °C.

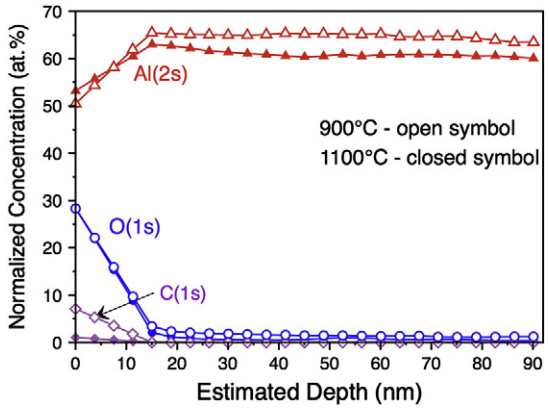

Fig. 8. XPS sputter depth profiles of 754 after aluminizing, the 900 °C (with powder) data are shown with open symbols and the 1100 °C data with closed symbols.

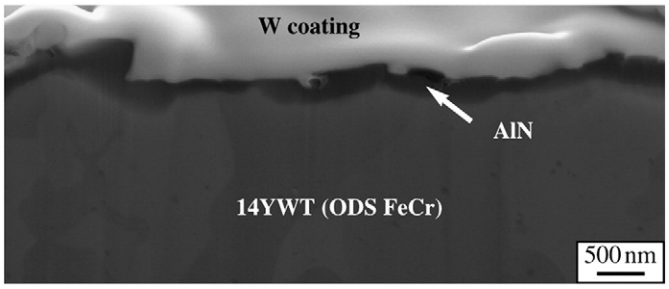

Fig. 11. SEM image of FIB cut cross-section of 14YWT after aluminizing at 1100 °C. The surface was coated with a layer of W for protection.

diffusion barrier preventing Al interdiffusion into the metal substrate during CVD aluminizing.

4. Discussion

The N content in 14YWT is the likely source of N to form the AlN layer as no nitride layer was observed on aluminized 754 or on other FM specimens. Table 1 shows that the nominal N content in 14YWT is more than 2× higher than levels in other FM steels. With their lower N levels, FM steels routinely form acicular AlN precipitates in the coating which coarsen with exposure time [24,31,33], but there has been no indication of a continuous surface layer as was observed for 14YWT specimens. The source of the AlN precipitates in aluminized FM steels was clearly shown to be the N in the alloy by coating studies on low-N model alloys [34]. Nickel-base alloy X was chosen for comparison because it also contains a relatively high N content, which did not inhibit aluminizing. However, the level in alloy X was 1/3 that in 14YWT and the grain size was much coarser, Table 1. A new Fe-base austenitic cast alloy, CF8C-Plus, has 9600 ppma N but was CVD aluminized at 900 °C without powder and formed a dense protective coating [35]. A slower N diffusion rate and higher solubility in the austenitic CF8C-Plus matrix may be the difference compared to 14YWT. The combination of high N content and fine grain size also may have increased the flux of N in 14YWT. The ODS 401 alloy, which aluminized similar to the FM alloys, had a lower N content than 14YWT and a fine grain size [28] but not as small as this batch of 14YWT, Table 1. The recrystallized ODS 754 alloy has a much larger primary grain size.

The reason 14YWT behaves differently than FM steels in aluminizing may be due to the combination of N and O in the alloy. Of course, all ODS alloys have high N and O contents compared to conventional alloys due to the nature of the powder metallurgy process used for fabrication, Table 1. However, even among ODS alloys, the N content in 14YWT was higher than expected which may have resulted in its

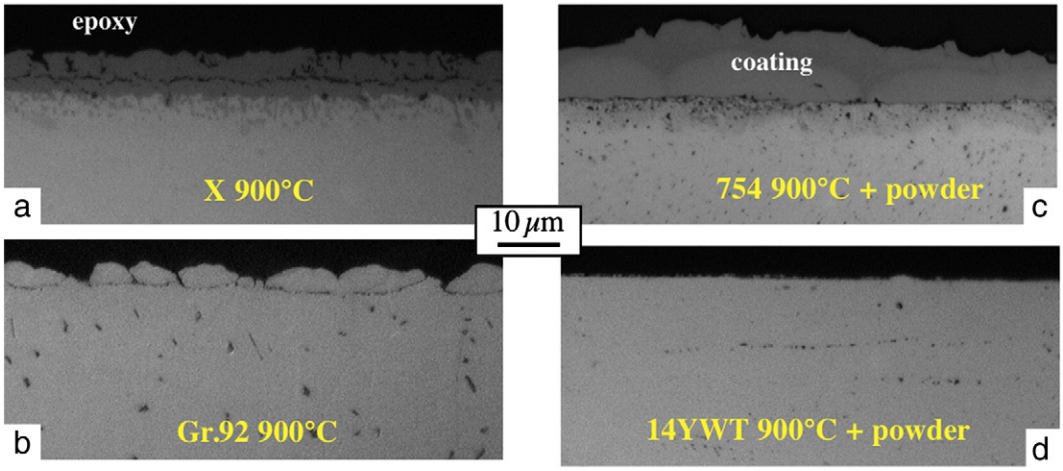

Fig. 9. Light microscopy of polished cross-sections after aluminizing for 6 h at 900 °C (a,b) without and (c,d) with Al–Cr powder, (a) alloy X, (b) alloy Gr.92, (c) alloy 754 and (d) 14YWT.

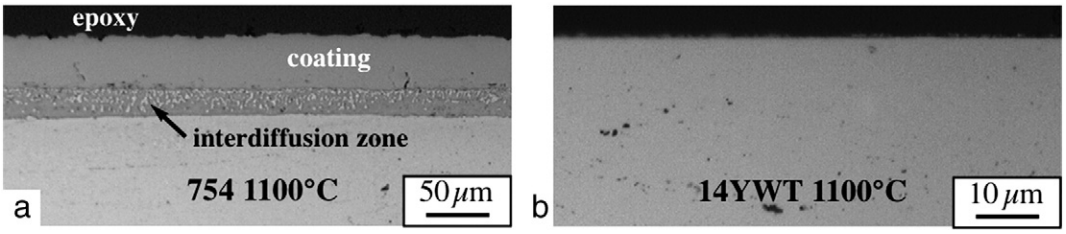

Fig. 10. Light microscopy of polished cross-sections after aluminizing for 6 h at 1100 °C (a) alloy 754 and (b) 14YWT.

unique behavior. Another reported unique aspect of 14YWT is the high density of Y–Ti oxide "nano-clusters" [36]. If the O distribution is different in 14YWT than other ODS alloys, the fine dispersion of oxide clusters may more readily allow the rapid formation of an Al-rich oxide layer in the CVD environment that could inhibit Al uptake in this alloy. Both XPS profiles in Fig. 6 suggest a high O concentration at the surface. After the Al-rich oxide layer forms, the high N content in the alloy could then react with Al forming the underlying AlN layer at a rate dependent on the temperature.

Fig. 1 clearly shows mass loss of uncoated 14YWT in Pb–Li at a similar rate as 401 and Gr.92. Thus, its maximum use temperature in a fusion reactor will be limited to ~500 °C by corrosion rather than creep or other properties. Batches of 14YWT with lower N content or larger grain size may be more amenable to coating. If the proposed mechanism for inhibiting aluminization is not correct, a different strategy may be needed for protecting 14YWT from dissolution in Pb–Li.

5. Summary

Prior work demonstrated the performance of Al-rich coatings made by chemical vapor deposition (CVD) on Grade 92 (Fe–9Cr–2W) and oxide dispersion strengthened (ODS) alloy 401 in inhibiting mass loss in isothermal Pb–Li capsule experiments. Specimens of ODS ferritic steel 14YWT were exposed in the same CVD reactor using similar conditions. However, the measured mass changes were extremely low compared to other wrought and ODS materials. After aluminizing at 900 °C with two Al activities and at 1100 °C, characterization showed that 14YWT formed a dense, primarily AlN layer that prevented Al uptake. The AlN surface formation during CVD aluminizing was attributed to the higher N content in this material than the other alloys. However, synergistic effects of the high O content and fine (~140 nm) grain size in 14YWT cannot be discounted. Future batches of this material with lower N contents need to be evaluated or another strategy used to mitigate mass loss in the presence of Pb–Li.

Acknowledgments

The authors would like to thank J. A. Haynes, K. M. Cooley, G. W. Garner, T. Lowe, H. Longmire, K. Unocic and H. Meyer for assistance with the experimental work. D. Hoelzer provided the 14YWT material and ODM 401 was provided by the manufacturer, Dour Metal sro, Slovak Republic. J. A. Haynes and K. A. Unocic provided helpful comments on the manuscript. This research was sponsored by the Office of Fusion Energy Sciences, U. S. Department of Energy (DOE).

References

[1] M. Abdou, D. Sze, C. Wong, M. Sawan, A. Ying, N.B. Morley, S. Malang, Fusion Sci. Technol. 47 (2005) 475.
[2] H. Tanigawa, K. Shiba, A. Möslang, R.E. Stoller, R. Lindau, M.A. Sokolov, G.R. Odette, R.J. Kurtz, S. Jitsukawa, J. Nucl. Mater. 417 (2011) 9.
[3] B.A. Pint, J.L. Moser, P.F. Tortorelli, Fusion Eng. Design 81 (2006) 901.
[4] B.A. Pint, J.L. Moser, P.F. Tortorelli, J. Nucl. Mater. 367–370 (2007) 1150.
[5] B.A. Pint, Mater. Sci. Forum 595–598 (2008) 549.
[6] B.A. Pint, J. Nucl. Mater. 417 (2011) 1195.
[7] B.A. Pint, L.R. Walker, K.A. Unocic, Mater. High Temp. 29 (2012) 129.
[8] J.E. Battles, Int. Mater. Rev. 34 (1989) 1.
[9] R.J. Lauf, J.H. DeVan, J. Electrochem. Soc. 139 (1992) 2087.
[10] P. Hubberstey, J. Nucl. Mater. 247 (1997) 208.
[11] T. Yoneoka, S. Tanaka, T. Terai, Mater. Trans. 42 (2001) 1019.
[12] J.H. DeVan, J. Nucl. Mater. 85–86 (1979) 249.
[13] S. Ukai, M. Fujiwara, J. Nucl. Mater. 307 (2002) 749.
[14] R.L. Klueh, J.P. Shingledecker, R.W. Swindeman, D.T. Hoelzer, J. Nucl. Mater. 341 (2005) 103.
[15] J. Konys, W. Krauss, J. Novotny, H. Steiner, Z. Voss, O. Wedemeyer, J. Nucl. Mater. 386–388 (2009) 678.
[16] H. Glasbrenner, Z. Peric, H.U. Borgstedt, J. Nucl. Mater. 233–237 (1996) 1378.
[17] H. Glasbrenner, J. Konys, Z. Voss, O. Wedemeyer, J. Nucl. Mater. 307–11 (2002) 1360.
[18] J. Konys, W. Krauss, Z. Voss, O. Wedemeyer, J. Nucl. Mater. 367–370 (2007) 1144.
[19] J.D. Fowler, R.A. Causey, D. Chandra, T.S. Elleman, K. Verghese, J. Vac. Sci. Technol. 13 (1976) 401.
[20] T. Sample, A. Perujo, H. Kolbe, B. Mancinelli, J. Nucl. Mater. 283–287 (2000) 1272.
[21] A. Aiello, A. Ciampichetti, G. Benamati, J. Nucl. Mater. 329–333 (2004) 1398.
[22] G.W. Hollenberg, E.P. Simonen, G. Kalinin, A. Terlain, Fusion Eng. Design 28 (1995) 190.
[23] W.Y. Lee, Y. Zhang, I.G. Wright, B.A. Pint, P.K. Liaw, Metall. Trans. A 29 (1998) 833.
[24] Y. Zhang, B.A. Pint, K.M. Cooley, J.A. Haynes, Surf. Coat. Technol. 202 (2008) 3839.
[25] N. Baluc, et al., J. Nucl. Mater. 417 (2011) 149.
[26] D.A. McClintock, M.A. Sokolov, D.T. Hoelzer, R.K. Nanstad, J. Nucl. Mater. 392 (2009) 353.
[27] T. Hayashi, P.M. Sarosi, J.H. Schneibel, M.J. Mills, Acta Mater. 56 (2008) 1407.
[28] H. Hadraba, L. Stratil, B. Kazimierzak and I. Dlouhy, submitted to J. Nucl. Mater.
[29] J.A. Haynes, B.A. Pint, K.L. More, Y. Zhang, I.G. Wright, Oxid. Met. 58 (2002) 513.
[30] B.A. Pint, J.A. Haynes, T.M. Besmann, Surf. Coat. Technol. 204 (2010) 3287.
[31] B.A. Pint, Y. Zhang, Mater. Corros. 62 (2011) 549.
[32] S.C. Kung, R.A. Rapp, Oxid. Met. 32 (1989) 89.
[33] A. Agüero, K. Spiradek, S. Hoefinger, M. Gutierrez, R. Muelas, Mater. Sci. Forum 595–598 (2008) 251.
[34] Y. Zhang, B.A. Pint, K.M. Cooley, J.A. Haynes, Surf. Coat. Technol. 200 (2005) 1231.
[35] P.J. Maziasz, B.A. Pint, J. Eng. Gas Turbines Power 133 (10) (2011) 102302.
[36] M.K. Miller, E.A. Kenik, K.F. Russell, L. Heatherly, D.T. Hoelzer, P.J. Maziasz, Mater. Sci. Eng. A 353 (2003) 140.